



# Gold Nanoparticle-Functionalized Diatom Biosilica as Label-Free Biosensor for Biomolecule Detection

Tongtong Chen<sup>1</sup>, Feifei Wu<sup>1</sup>, Yang Li<sup>2</sup>, Hussein E. Rozan<sup>1,3</sup>, Xiguang Chen<sup>1,4</sup> and Chao Feng<sup>1\*</sup>

<sup>1</sup>College of Marine Life Science, Ocean University of China, Qingdao, China, <sup>2</sup>College of Life Sciences, Qingdao University, Qingdao, China, <sup>3</sup>Department of Biochemistry, Faculty of Agriculture, Al-Azhar University, Cairo, Egypt, <sup>4</sup>Qingdao National Laboratory for Marine Science and Technology, Qingdao, China

## OPEN ACCESS

### Edited by:

Junchao Wei,  
Nanchang University, China

### Reviewed by:

Jichang Han,  
Ningbo University, China  
Piwu Li,  
Qilu University of Technology, China

### \*Correspondence:

Chao Feng  
fengchao@ouc.edu.cn

### Specialty section:

This article was submitted to  
Biomaterials,  
a section of the journal  
Frontiers in Bioengineering and  
Biotechnology

**Received:** 12 March 2022

**Accepted:** 21 April 2022

**Published:** 27 May 2022

### Citation:

Chen T, Wu F, Li Y, Rozan HE, Chen X  
and Feng C (2022) Gold Nanoparticle-  
Functionalized Diatom Biosilica as  
Label-Free Biosensor for  
Biomolecule Detection.  
*Front. Bioeng. Biotechnol.* 10:894636.  
doi: 10.3389/fbioe.2022.894636

Diatom biosilica (DBs) is the cell wall of natural diatom called frustule, which is made of porous hydrogenated amorphous silica possessing periodic micro- to nanoscale features. In this study, a simple, sensitive, and label-free photoluminescence (PL) immune-detection platform based on functionalized diatom frustules was developed. Gold nanoparticles (AuNPs) deposited on poly-dopamine-coated diatom frustules *via in situ* deposition which considerably decreased the intrinsic blue PL intensity of diatom biosilica. Then, goat anti-rabbit immunoglobulin G (IgG) was added to functionalize diatom biosilica-poly-dopamine-AuNPs (DBs-PDA-AuNPs). PL studies revealed that the specific binding with antigen rabbit IgG increased the peak intensity of PL in comparison with the non-complimentary antigen (human IgG). The enhancement in PL intensity of DBs-PDA had a linear correlation with antigen (rabbit IgG) concentration, whose limit of detection (LOD) reached  $8 \times 10^{-6}$  mg/ml. Furthermore, PL detection based on DBs-PDA-AuNPs showed a high detection sensitivity with the LOD as low as  $8 \times 10^{-9}$  mg/ml and spread over almost eight orders of magnitude, making it suitable for the sensitive quantitative analysis of immune complex compared with traditional fluorescence immunoassay. Hence, the study proves that the AuNP-functionalized diatom frustules can serve as an effective biosensor platform for label-free PL-based immunoassay.

**Keywords:** antibody, biosensor, diatom, biosilica, photoluminescence, gold nanoparticles

## 1 INTRODUCTION

Immuno-detection *via* special recognition with antibody-antigen is an essential tool for clinical detection and diagnosis of diseases rapidly and reliably (Uram et al., 2006; Lin et al., 2013). Compared to electrical and mass measurement methods, optical biosensors have attracted much attention because of their high sensitivity, specificity, and convenience (Dong et al., 2015; Peltomaa et al., 2018; Wang et al., 2019). Label-based optical biosensor such as fluorescence bio-sensing has been widely used in immunoassay, but the photo-bleaching and the limitation of multiplex detection are normally along with the contamination of the sample matrix due to the introduction of labels, which restricts its application in clinic (Gale et al., 2009). Label-free optical bio-sensing platforms can offer real-time monitoring of immune-complex and avoid these drawbacks mentioned earlier (Viji et al., 2014). Surface plasmon resonance (SPR) is one of the most used label-free optical biosensors whose plasmon mode will change when biomolecules bind to the surface of a metal film (Meyer et al.,

2011). However, there is a challenge for SPR sensor to detect small biomolecules, such as antibodies, since the binding of small size molecules changes little the refractive index, which reduces the sensitivity of the measurement. On the other hand, the signal uniformity and reproducibility of surface-enhanced Raman spectroscopy (SERS) for small molecules detection, for example, aptamers and antibodies, also confine its uses in the laboratory (Kashif et al., 2020).

Diatoms are mono-cellular eukaryotic phytoplankton widely distributed in oceans and lakes. Diatoms take up soluble silicon to form the cell wall of amorphous silica, which possesses three-dimensional micro- to nano-porous structures (Gordon et al., 2009; De Tommasi et al., 2013). Several studies found that DBs possessed unique photoluminescence (PL) properties which changed upon different biomolecules depositing on its surface, which revealed their promising applications in optical biosensing without labeling (Qin et al., 2008; De Tommasi, 2016; LeDuff et al., 2016; Mishra et al., 2020). The PL property of DBs was induced by various surface groups on DBs including Si-OH, Si-H groups, non-bridging oxygen hole centers, and self-trapped excitons (He et al., 2004). Nucleophilic biomolecules such as antibodies enhanced the PL peak intensity by donating electrons to non-radiative defect sites on DBs (Gale et al., 2009; Viji et al., 2014). Within the past few years, DBs has been developed as label-free bio-sensing platforms of PL-based gas sensors for detecting small biomolecules, such as antibodies and explosive derivatives (Viji et al., 2014; Rea et al., 2016; Zhen et al., 2016).

Considering the definite limitations of DBs in immunoassay due to its unreactive nature of the surface, Gregory and his colleagues introduced  $-NH_2$  on DBs by reaction with 3-aminopropyltrimethoxysilane (APS) and then covalently attached with rabbit immunoglobulin G (IgG) (Gale et al., 2009). The special binding between rabbit IgG with the complimentary antigen goat anti-rabbit IgG increased the PL peak intensity by at least three times in comparison with bare DBs. Furthermore, the enhancement in PL intensity with antigen (goat anti-rabbit IgG) concentration was displayed by a Langmuir model for immune-complex formation. De Stefano et al. (2009) also utilized APTS to modify DBs, using the PL of *Coscinodiscus concinnus* for quantitative analysis and detection of proteins. Zhen et al. (2016) found that the PL emission was partially quenched when TNT binding to the anti-TNT ScFv-functionalized DBs. These results validate that DBs can be used as an optical biosensor platform for PL-based immunoassay. Aforementioned strategies are all based on chemical modification. Poly-dopamine (PDA) can coat the surface of DBs in virtue of its great adhesive properties which is considered an environmentally friendly method for the surface modification of DBs (Uthappa et al., 2019). PDA coating can promote antibody functionalization by virtue of its adhesion properties. In addition, PDA coating can improve the sensitivity of diatoms PL detection by reducing the defect concentration of DBs. Therefore, we used PDA to modify DBs to make it a better optical biosensor based on PL detection.

Noble metal nanoparticles such as gold nanoparticles (AuNPs) and silver nanoparticles (AgNPs) exhibit unique optical properties. They can display the localized surface plasmon resonance (LSPR)

phenomenon, whose absorbance will be light very intense when excited at certain wavelengths (Ren et al., 2013; Liu et al., 2018; Petzold and Zollfrank, 2019). According to the surface state luminescence model proposed by Xie et al. (1992), the deposition of metal nanoparticles on the surface of DBs change its surface state and cause its PL intensity to decay. Thus, AuNPs may have the potential to be used in optical biosensors based on PL. In addition, AuNPs possess advantages of being easy to synthesize and modify, good stability, and biocompatibility (Leng et al., 2010). On the other hand, AuNPs possessing ultra-small sizes bound and assemble on the surface of DBs, increasing the available surface area of binding biomolecules and enhancing optical signal sensitivity. Therefore, the deposition of AuNPs on DBs can serve as substrates for optical biosensors.

In this study, we utilized PDA and AuNP-functionalized DBs (Scheme 1). Then, the antibody goat anti-rabbit IgG was attached to PDA coated on DBs (DBs-PDA) and AuNPs deposited on DBs-PDA (DBs-PDA-AuNPs). We examined the correlation of antibody goat anti-rabbit IgG-functionalized DBs-PDA and DBs-PDA-AuNPs with antigen rabbit IgG concentrations in the range from  $8 \times 10^{-9}$  to  $8 \times 10^{-2}$  mg/ml. DyLight 488-labeled rabbit IgG was employed for immunoassay to compare with the PL and fluorescence detection. Furthermore, in order to validate the universality of DBs as a photo-luminescent immune-sensor, we detected the correlation between the PL peak intensity of rabbit anti-human IgG-functionalized DBs-PDA and DBs-PDA-AuNPs and different concentrations of human IgG (from  $8 \times 10^{-9}$  to  $8 \times 10^{-2}$  mg/ml). In conclusion, PL detection based on DBs-PDA-AuNPs can be applied to the selectivity, high sensitivity, and label-free immunoassay.

## 2 MATERIALS AND METHODS

### 2.1 Reagents and Materials

NaOH, bovine serum albumin (BSA), and dopamine hydrochloride (DA) were all purchased from Sigma-Aldrich (United States), and 0.2 M phosphate-buffered saline (PBS) (pH 7.4) was prepared by mixing the stock solutions of  $KH_2PO_4$  and  $K_2HPO_4$ .  $HAuCl_4 \cdot 3H_2O$  was purchased from Shanghai Aladdin Biochemical Technology Co., Ltd. Rabbit IgG (RIgG), human IgG (HIgG), goat anti-rabbit IgG (GaR), DyLight 488-rabbit IgG (DyLight 488-RIgG), and rabbit anti-human IgG (RaH) were all purchased from Wuhan Boster Biological Technology Ltd. *C. cryptica* (GY-H32) was obtained from the Key Laboratory of Marine Genetics and Breeding, Ocean University of China.

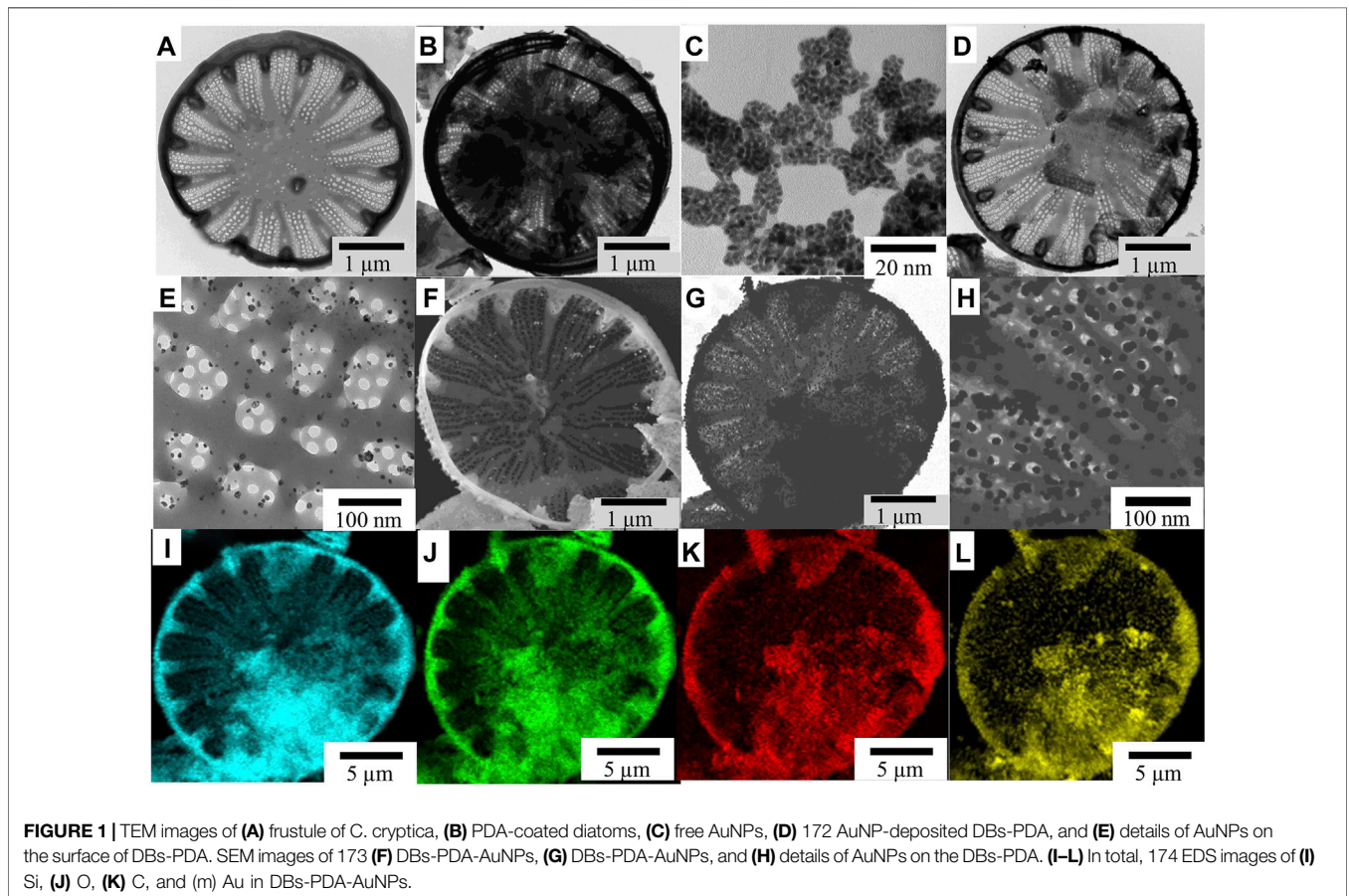
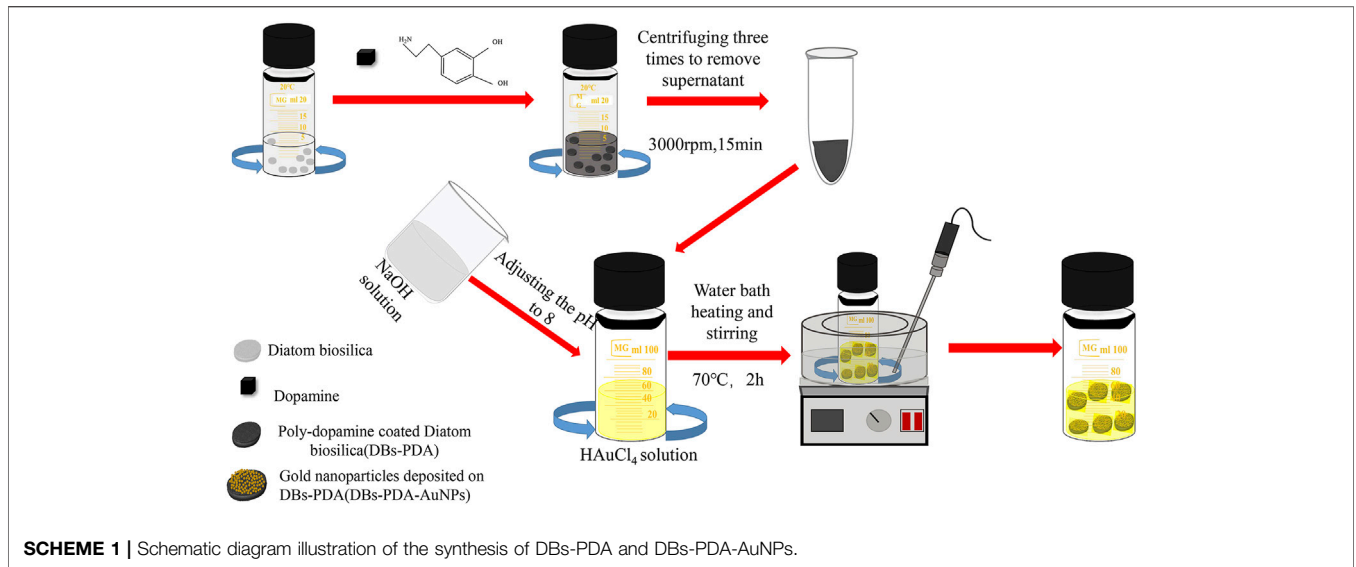
### 2.2 Preparation of Diatom Biosilica

#### 2.2.1 Cultivation of Diatom

*C. cryptica* was cultured in F/2 medium at 20°C with an alternating light/night cycle of 12:12 h for 2 weeks. The diatom cells were obtained *via* filtration and washed three times using deionized water.

#### 2.2.2 Treatment of Diatom Frustules

*C. cryptica* of 25 g was mixed with 50 ml lye (potassium hydroxide: urea: water = 16:8:66) and stirred evenly, repeated



freezing (under  $-25^{\circ}\text{C}$  for 5–6 h each time) and thawing twice frozen twice, and rinsed several times. Then, the pre-cooled treated sample was added to 50 ml of chilled piranha solution (sulfuric acid: hydrogen peroxide = 7:3), which was subsequently

heated in a water bath of  $75^{\circ}\text{C}$  for 30 min and stirred constantly, followed by cooling, diluting once, washing by centrifugation several times, and drying in the oven to obtain DBs with the hierarchical porous structure (Figure 1A).

## 2.3 Dopamine Coating on DBs

DBs of 10 mg was dissolved in 10 ml deionized water and stirred continuously for 40 min. Then, 40 mg dopamine hydrochloride (DA) and 200  $\mu$ l NaOH solution (0.1 M, 50 ml) were added into the diatom solution and stirred evenly. Dopamine hydrochloride (DA) is self-polymerized to poly-dopamine (PDA) in a weak alkaline environment. Then, the sample was centrifuged (3,000 rpm, 15 min) three times, and the supernatant was removed. DBs coated by PDA (DBs-PDA) could be observed using the transmission electron microscope (Figure 1B).

## 2.4 Synthesis of AuNP-Functionalized DBs-PDA

AuNPs were fabricated by the modified method reported previously (Jia et al., 2005). Chloroauric acid ( $\text{HAuCl}_4 \cdot 3\text{H}_2\text{O}$ ) of 85 mg was dispersed in 50 ml ultrapure water and adjusted the pH to 8.0 with 0.1 M NaOH solution. Next, the obtained DBs-PDA was added, heated to 70°C, and continuously stirred for 2 h. Afterward, the resulting solution mixture was centrifuged (3,000 rpm, 15 min) until the absence of  $\text{Cl}^-$  ion and removed the supernatant. Finally, the precipitates were dried completely in the oven.

## 2.5 Preparation of Immuno-Sensors

### 2.5.1 Immobilization of Antibody on DBs-PDA-AuNPs

DBs functionalized with antibody was prepared by following the methods reported previously (Lai et al., 2013). First, DBs-PDA-AuNP (1.5 mg/ml) suspension was adjusted to the pH 9.0 with 0.1 M  $\text{K}_2\text{CO}_3$ . Then, 30  $\mu$ l goat anti-rabbit IgG was added to 50  $\mu$ l suspension, by gently mixing at room temperature for 2 h. The sample was then centrifuged for 15 min, followed by mixing with 5% BSA for 1 h for blocking, and washing with PBS twice successively. After centrifugation, antibody-conjugated diatom frustules were collected and re-dissolved in 0.5 ml PBS containing 0.1% BSA. The resulting product was then stored at 4°C for further use.

### 2.5.2 Immunological Reactions

Stocked antigens were prepared by mixing 10  $\mu$ l RIgG (with the concentration of 10 mg/ml) with 990  $\mu$ l PBS. Then, 100  $\mu$ l DBs-PDA-AuNPs-GaR and RIgG with the concentrations ranging from  $8 \times 10^{-9}$  to  $8 \times 10^{-2}$  mg/ml were dissolved in a polystyrene 12-well plate containing 2 ml PBS, which was then gently mixed for 2 h at room temperature.

## 3 RESULTS AND DISCUSSION

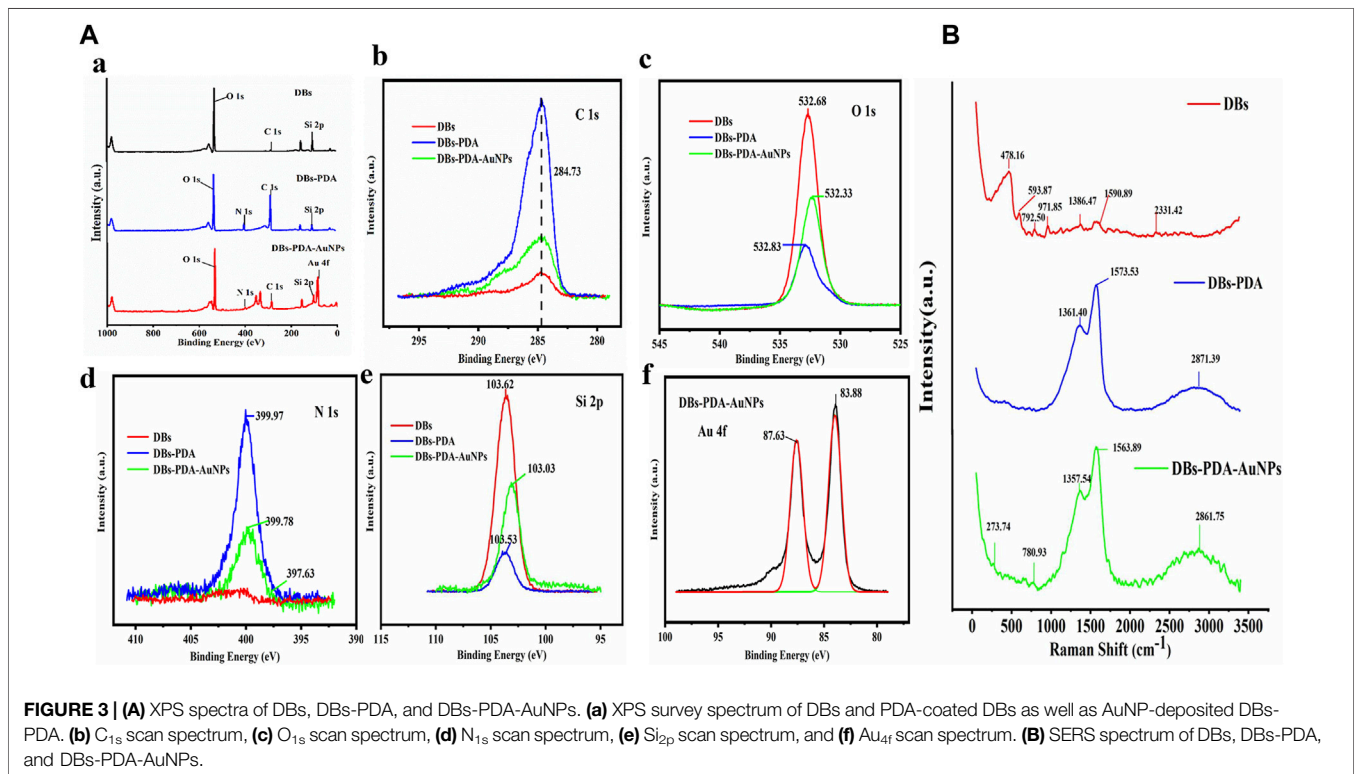
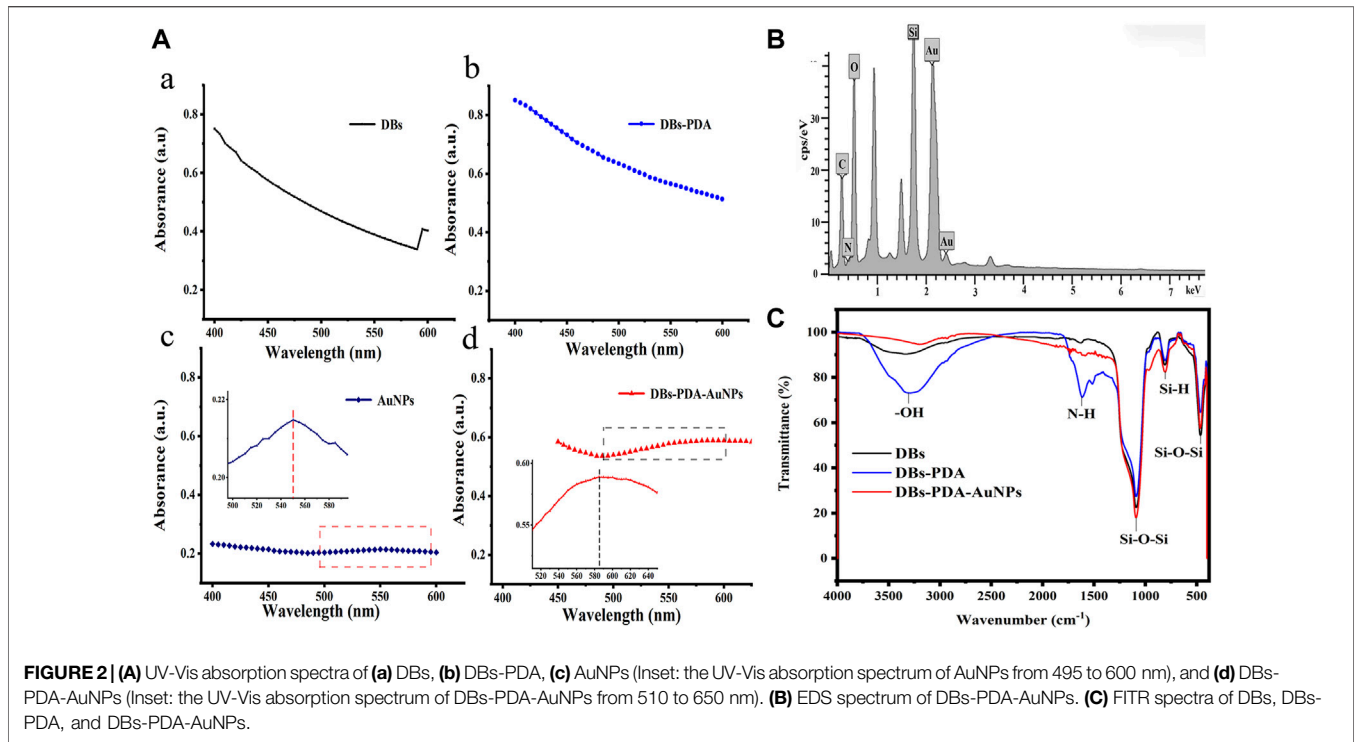
### 3.1 Synthesis and Characterization of DBs-PDA-AuNPs

DBs was isolated from cultured *C. cryptica* using chilled piranha solution to remove the organic matter in cells. The purified DBs was drum-shaped with a diameter of 10~30  $\mu$ m and possessed a hierarchical pore structure (Figure 1A). After mixing DBs and DA under weak alkaline conditions (Scheme 1), DA could be oxidized spontaneously, and PDA coating was formed

(Figure 1B) via the self-polymerization-crosslinking reaction on the surface of DBs. AuNPs were likely to self-assemble with regular size and shape on the surface of DBs-PDA via in situ deposition (Figures 1D, F, G). The free AuNPs were 3~5 nm diameter and aggregated to form clusters (Figure 1C). In contrast, the AuNPs on DBs-PDA-AuNPs were agglomerated for a larger size with a diameter of 15~20 nm and distributed evenly on the surface of DBs (Figure 1G). This might be explained by the higher agglomeration tendency of AuNPs when depositing on DBs. EDS images validated that elements of Si (Figure 1I), O (Figure 1J), C (Figure 1K), and Au (Figure 1L) could be found on DBs-PDA-AuNPs which also confirmed the successful immobilization of AuNPs on DBs.

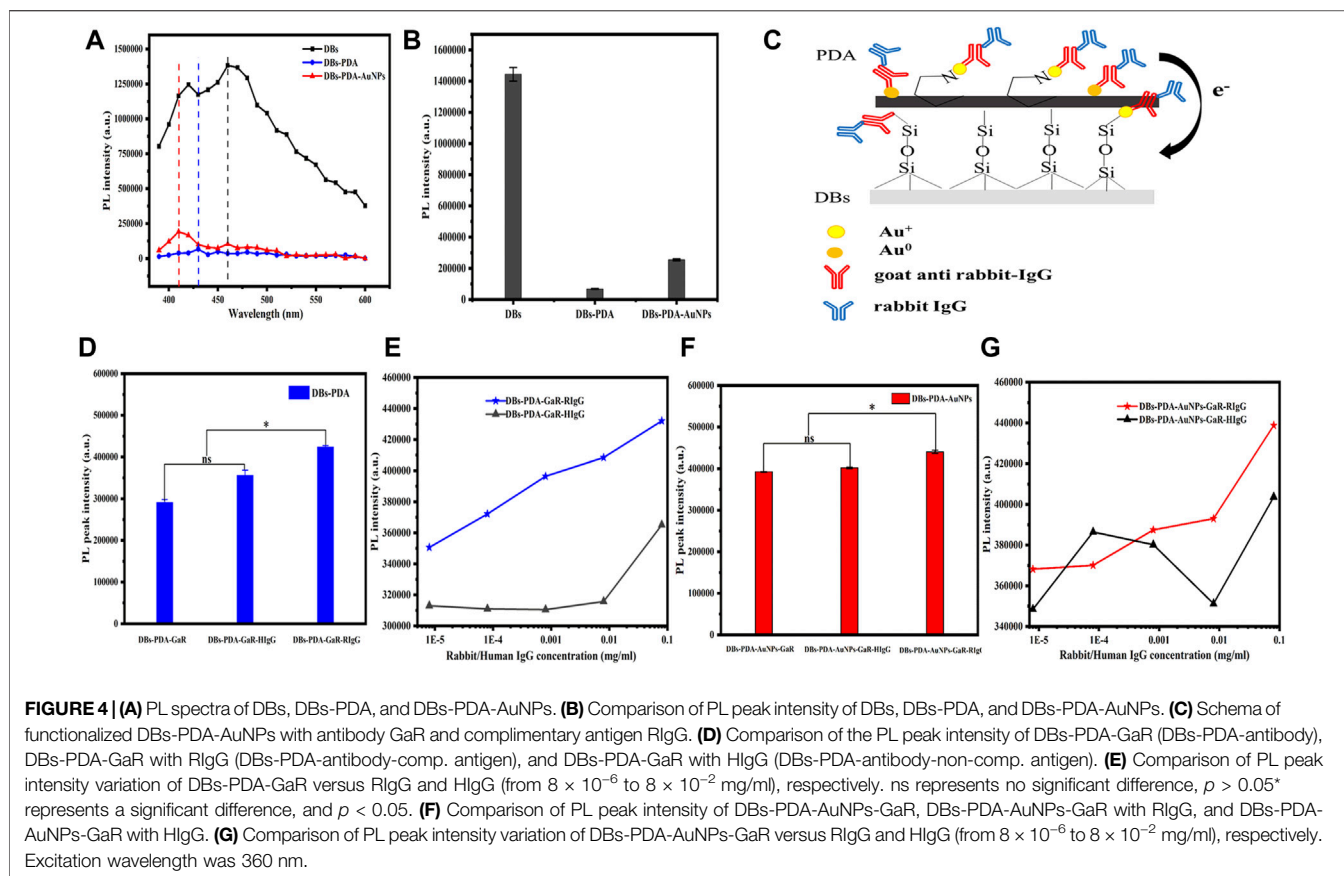
The UV-Vis spectra of DBs, DBs-PDA, AuNPs, and DBs-PDA-AuNPs showed that there were no characteristic absorption peaks in the spectra of DBs and DBs-PDA at the wavelength range of 400~600 nm, and their spectral shapes were very similar (Figure 2A,B). The noticeable characteristic absorption band peaking at 550 nm, which was an indicative of the formation of AuNPs, was observed in the UV-Vis spectrum (Figure 2C). After AuNPs deposited on the surface of DBs-PDA, the absorption peak intensity of DBs-PDA-AuNPs increased in comparison with AuNPs alone. The absorption band of DBs-PDA-AuNPs was red-shifted and the peak appeared at about 580 nm, indicating the aggregation of AuNPs on DBs-PDA (Figure 2d), which was consistent with the agglomeration tendency observed in the SEM image (Figure 1H). The energy dispersive X-ray spectrum (EDS) of DBs-PDA-AuNPs presented the distribution of elements including C, O, Si, and Au and further validated the existence of AuNPs (Figure 2B). The FT-IR spectra clearly showed characteristic peaks for DBs, including Si-O-Si bending at 466 and 806  $\text{cm}^{-1}$ , Si-O-Si stretching at 1,090  $\text{cm}^{-1}$ , and O-H stretching of surface-bound hydroxyl groups at 3,147  $\text{cm}^{-1}$ , which mainly included bound water, H-O-Si, and pyrocatechol of poly-dopamine. After PDA coated on DBs, the strong peaks at 1,615  $\text{cm}^{-1}$  shown in the spectrum corresponded to the typical absorption peak of amide bonds on the PDA chain (Yang et al., 2014). However, when AuNPs deposited on DBs-PDA, the amide bonds almost disappeared, which might suggest the formation of Au-N. According to the infrared spectra, the characteristic absorption peak at  $-3,147 \text{ cm}^{-1}$  weakened after AuNPs functionalized DBs, suggesting that the free Si-OH on DBs reacted with AuNPs to form the Si-O-Au group (Figure 2C). From the aforementioned results, it could be concluded that AuNPs had been successfully fixed on the surface of DBs-PDA.

The XPS survey spectrum indicated that AuNPs were successfully deposited on the surface of DBs (Figure 3A). The functionalization of PDA coating and AuNPs only displays a peak C1s at 284.73 eV (Figure 3B). After AuNPs deposited on DBs, the two components of Au 4f<sub>7/2</sub> were at binding energy = 83.9 and 87.6 eV, which indicated the emergence of Au<sup>0</sup> and the ion of Au<sup>+1</sup> on the surface of DBs-PDA-AuNPs, respectively. This result demonstrated that the chloroauric acid was reduced to AuNPs and successfully immobilized on DBs-PDA (Figure 3f). The appearance of the N<sub>1s</sub> peak of DBs-PDA and DBs-PDA-AuNPs near 399 eV could be attributed to the existence of NSi<sub>2</sub>O (Figure 3d). The Si<sub>2p</sub> of DBs located at 103.62 eV was



attributed to SiO<sub>2</sub>, and the peak value of DBs-PDA was shifted toward a lower binding energy around 0.09 eV (from 103.6 to 103.5 eV), implying that part of the Si-OH bond had been

transferred into Si-N bond. In addition, the Si<sub>2p</sub> of DBs-PDA-AuNPs located at 103.0 eV was shifted to lower binding energy by 0.5 eV than that of DBs-PDA, suggesting that part of the Si-N



bond had changed to Si–Au bond (Figure 3e). Thus, AuNPs were more likely to form Si–O–Au bonds with the free Si–OH on the surface of DBs.

The Raman spectrum of DBs had a characteristic peak at  $478.2 \text{ cm}^{-1}$ , corresponding to Si–O–Si stretching vibration (red curve). Due to the introduction of PDA, peaks of  $-1,362$  and  $-1,571 \text{ cm}^{-1}$  of DBs-PDA and DBs-PDA-AuNPs both appeared in the Raman spectra which were attributed to the presence of aromatic phenyl in PDA (blue and green curves). The characteristic absorption peak at  $2,850\text{--}2,923 \text{ cm}^{-1}$  was attributed to the stretching vibration of  $-\text{CH}$ . DBs-PDA-AuNPs (green curve) had a weak characteristic peak at  $-270 \text{ cm}^{-1}$  which did not appear in the Raman spectra of DBs and DBs-PDA (red and blue curve) (Figure 3b). It was supposed that this characteristic absorption peak was concerned with the formation of N–Au (Figure 4C). The aforementioned results showed that when AuNPs were deposited on the surface of DBs-PDA, PDA chelated Au (I) *via* catechol and amino groups. Therefore, AuNPs were immobilized on the surface of DBs-PDA.

## 3.2 PL Studies

### 3.2.1 PL Detection of DBs-PDA-AuNPs

The PL properties of DBs, DBs-PDA, and DBs-PDA-AuNPs were evaluated using the multimode microplate reader. Several studies have demonstrated that DBs have intrinsic blue photoluminescence due to the surface defects on the DBs, (Rorrer et al., 2007; Arteaga-

Larios et al., 2014; De Tommasi, 2016) which was also confirmed by our studies. It was observed that bare DBs emitted strong blue photoluminescence centered at 450 nm when samples were excited at 360 nm (Figure 4A). After being coated by PDA, the PL intensity of DBs-PDA was violently quenched, which displayed 13-fold lower than that of bare DBs (Figure 4B). The peak wavelength for DBs-PDA exhibited a blue shift from 450 to 430 nm caused by the interaction of PDA and the surface of DBs (Figure 4A). Defect concentration affected the PL properties of DBs. Thus, the decreased PL peak intensity and blue shift of DBs-PDA might be ascribed to the reduction of defect concentration when there is existence of PDA coating on the surface of DBs. Fedorenko et al. (2020) reported the similar results that PDA coating on ZnO nanorods caused the decrease of the defect concentration and the PL peak intensity. The PL emission spectra clearly showed 6-fold weaker PL peak intensity of DBs-PDA-AuNPs than that of bare DBs (Figure 4B). AuNPs functionalized DBs by forming Si–O–Au bonds, which induced the emergence of a new non-radiative center on the surface of DBs and decreased the PL peak intensity of DBs-PDA-AuNPs. The PL spectrum of DBs-PDA-AuNPs showed an obvious blue shift (from 450 to 410 nm). This result highlighted that AuNPs deposited on DBs *via in situ* polymerization would lead to the blue shift of the peak position. However, the PL peak intensity of DBs-PDA-AuNPs was one-fold higher than that of DBs-PDA. It was supposed that  $\text{Au}^+$ , which was formed by  $\text{Au}^{3+}$  reduction, combined with amino functional groups of PDA on the surface of DBs-PDA-

AuNPs to form N–Au bonds. The interaction between AuNPs and PDA induced the enhancement of surface passivation on DBs-PDA-AuNPs, which affected the surface recombination centers, the radiative points responsible for the PL of DBs. This inference could explain the rise of PL peak intensity after AuNPs functionalized DBs-PDA compared with DBs-PDA alone (Figure 4C).

### 3.2.2 Specificity

Our experiments validated the specificity of antibody-functionalized DBs-PDA-AuNPs with its complementary antigen. First, when GaR-functionalized DBs-PDA (DBs-PDA-GaR) bonds with non-complementary antigen HIgG, the PL peak intensity of DBs-PDA-GaR-HIgG showed no significant change. However, when the complementary antigen RIgG bound with DBs-PDA-GaR, the PL peak intensity was significantly different ( $p < 0.05$ ) which increased by more than 45% than that of DBs-PDA-GaR alone. (Figure 4D). The PL peak intensity of the formed complex between RIgG and GaR-functionalized DBs-PDA-AuNPs (DBs-PDA-AuNPs-GaR) changed significantly ( $p < 0.05$ ) which increased more than 12% than DBs-PDA-AuNPs-GaR. However, no significant change in the PL peak intensity was observed after DBs-PDA-AuNPs-GaR functionalized with non-complementary antigen HIgG (Figure 4F). The reason behind the peak PL intensity increase of the immune complex was the forming of nucleophilic molecules on the surface of DBs that transferred electrons to non-radiative defect sites on DBs (Figure 4C). In immune complex formation, the PL intensity of antibody binding on DBs-PDA-GaR and DBs-PDA-AuNPs-GaR showed a linear increase with the antigen RIgG concentration ranging from  $8 \times 10^{-6}$  to  $8 \times 10^{-2}$  mg/ml whereas non-complementary antigen HIgG did not (Figures 4E,G). These results illustrated the specificity of DBs-PDA and DBs-PDA-AuNPs applied to immune-detection.

### 3.4 RIgG Detection Based on DBs-PDA-AuNPs

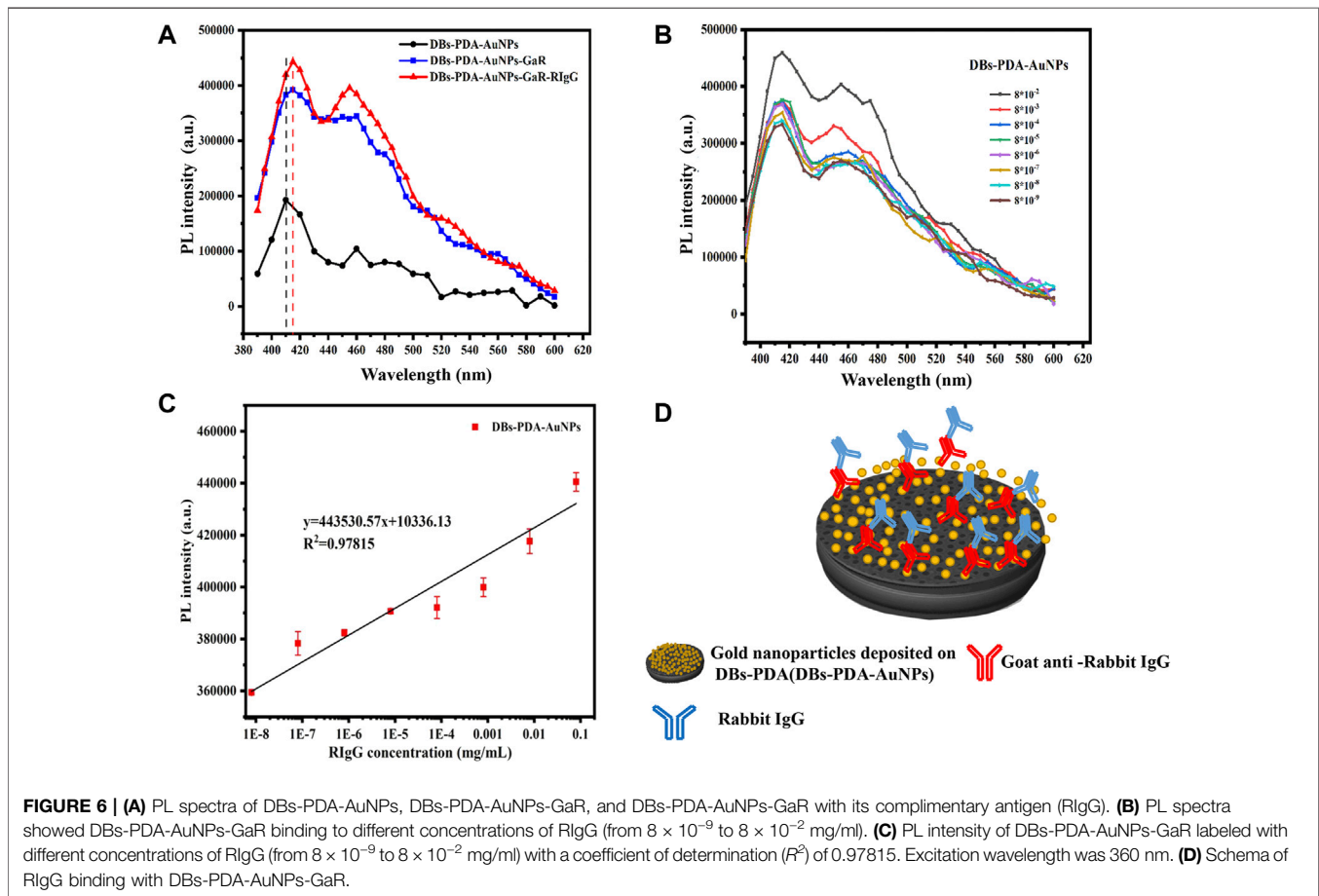
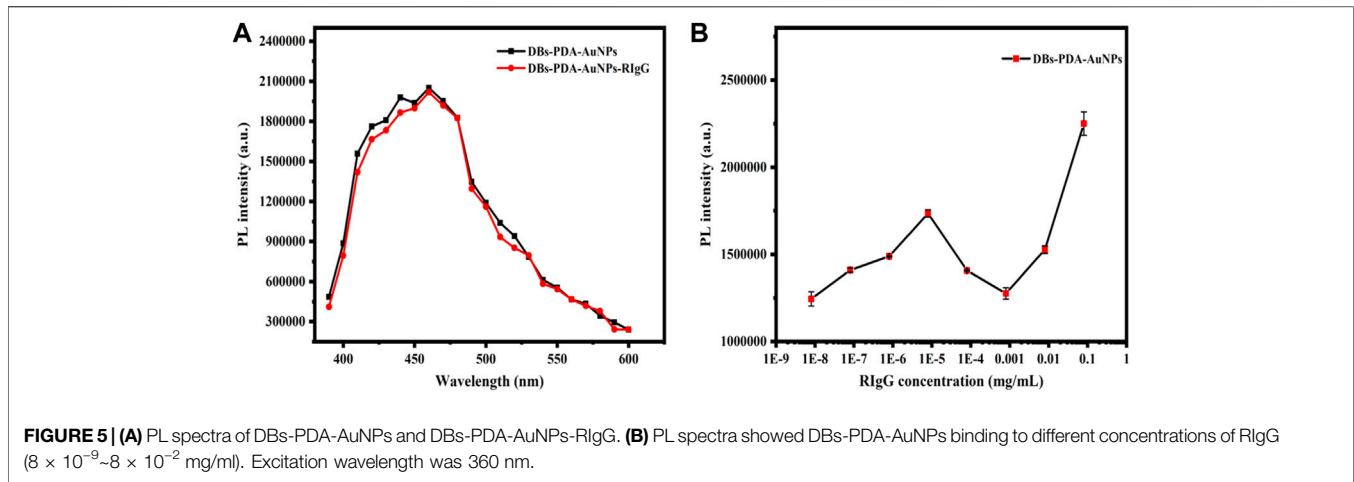
According to PL spectra of DBs-PDA-AuNPs and DBs-PDA-AuNPs-RIgG, when RIgG functionalized DBs-PDA-AuNPs, its peak PL intensity basically did not change compared with DBs-PDA-AuNPs, and the characteristic absorption peak did not change either (Figure 5A). As the concentration of RIgG changed (from  $8 \times 10^{-9}$  to  $8 \times 10^{-2}$  mg/ml), the peak PL intensity of DBs-PDA-AuNPs-RIgG did not show a linear relationship with the concentration change (Figure 5B). These results indicated that RIgG did not bind to the surface of DBs through reaction with AuNPs. A minute quantity of RIgG deposited on DBs, which would not affect the PL property of DBs-PDA-AuNPs. However, after GaR functionalized DBs-PDA-AuNPs, the peak PL intensity was 2-fold as that of DBs-PDA-AuNPs. In addition, the enhancement of defect concentration on the surface of DBs-PDA-AuNPs-GaR contributed to a slight blue shift of the PL characteristic peak (from 410 to 415 nm). Furthermore, the specific binding between GaR and its complementary antigen RIgG induced the PL intensity, with a 10% increase in comparison with DBs-PDA-AuNPs-GaR, and more than one-fold higher than that of DBs-

PDA-AuNPs (Figure 6A). These results confirmed that the nucleophilic complex attaching to DBs could increase PL intensity. The PL emission spectra of DBs-PDA-AuNPs showed that the peak PL intensity was linearly increased with RIgG concentrations in the range of  $8 \times 10^{-9}$  to  $8 \times 10^{-2}$  mg/ml without any peak shifts (Figure 6B). The increase in PL peak intensity with various RIgG concentrations was described by the best-fit equation:  $y = 443530.57x + 1.03E04$  and the coefficients of determination ( $R^2$ ) of 0.9781 (Figure 6C). These results illustrated that antigen RIgG molecules were adsorbed on the surface of DBs-PDA-AuNPs-GaR and involved in the formation of immuno-complex (Figure 6D). As a platform of immuno-detection, DBs-PDA-AuNPs showed an outstanding PL performance for detecting RIgG with the LOD reaching as low as  $8 \times 10^{-9}$  mg/ml.

For DBs-PDA groups, the PL emission spectra clearly indicated that the PL peak intensity of RIgG-functionalized DBs-PDA (DBs-PDA-RIgG) barely changed and without any peak shift as compared to that of DBs-PDA alone (Figure 7A). Furthermore, there was no linear relationship between the PL peak intensity and RIgG concentrations (from  $8 \times 10^{-9}$  to  $8 \times 10^{-2}$  mg/ml) (Figure 7B). This indicated that RIgG did not react with the free groups on the surface of DBs-PDA, and only a small amount of RIgG was deposited on DBs-PDA. Thus, the PL performance of DBs-PDA-RIgG was consistent with that before RIgG deposition. When RIgG bonds with DBs-PDA-GaR (Figure 8D), the PL peak intensity was enhanced by more than 10%, and a slight blue peak shift could be observed in PL emission spectra which was due to the decrease of defect concentration on the surface of DBs-PDA (Figure 8A). In immune-complex formation, the PL peak intensity showed a linear increase with concentrations of the complementary antigen RIgG from the range of  $8 \times 10^{-6}$  to  $8 \times 10^{-2}$  mg/ml (Figure 8B). The PL emission spectra clearly showed the increase in PL peak intensity with various RIgG concentrations (from  $8 \times 10^{-9}$  to  $8 \times 10^{-2}$  mg/ml). However, the peak PL intensity of DBs-PDA was found to be increasing linearly with the RIgG concentrations from  $8 \times 10^{-6}$  to  $8 \times 10^{-2}$  mg/ml. The regression equation was  $y = 19373.31x + 4.49E05$  with the correlation coefficient of determination ( $R^2$ ) of 0.99026 (Figure 8C). The limit of PL detection for RIgG based on DBs-PDA reached  $8 \times 10^{-6}$  mg/ml, which was three orders of magnitude lower than that of DBs-PDA-AuNP-based detection.

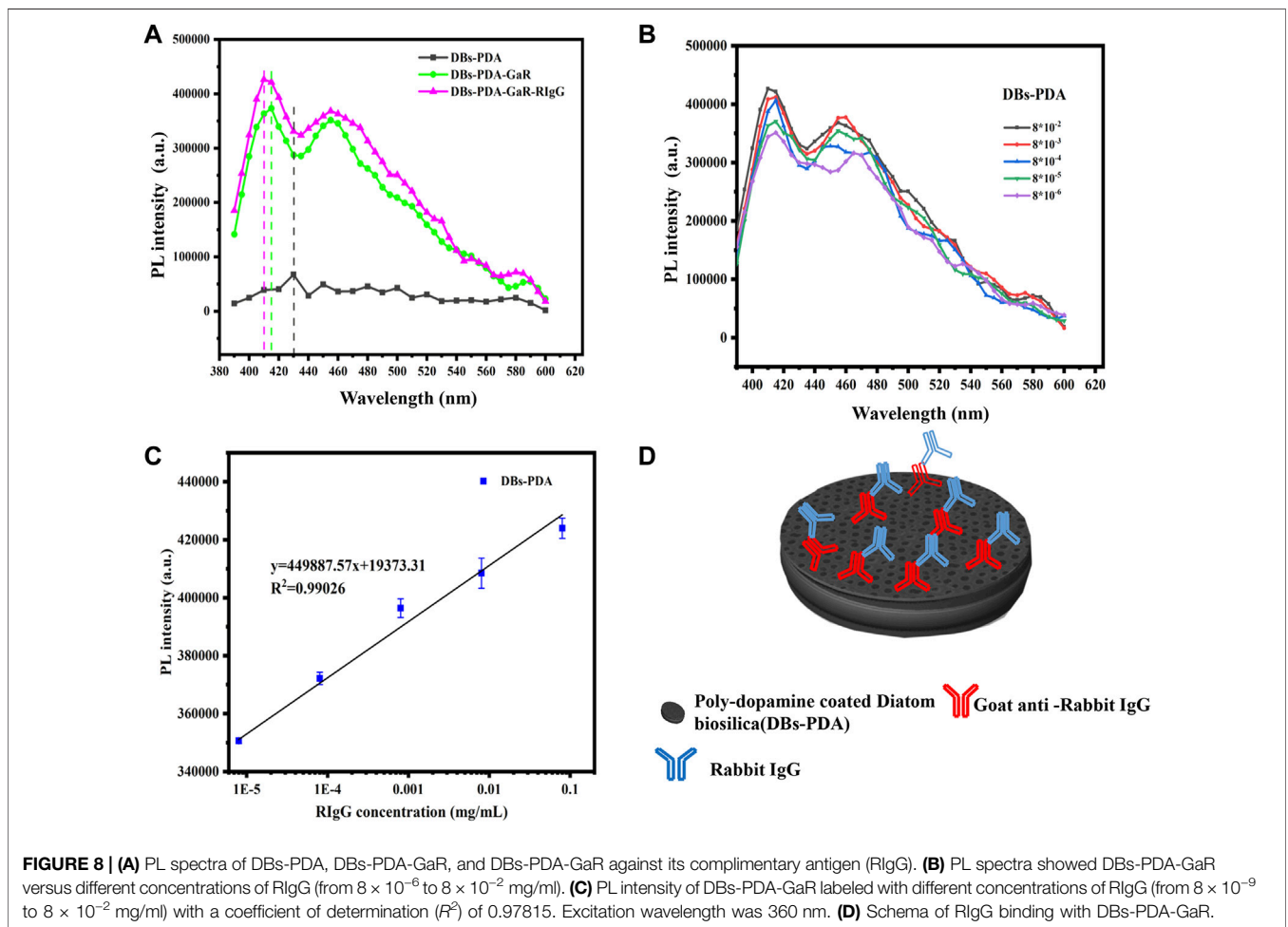
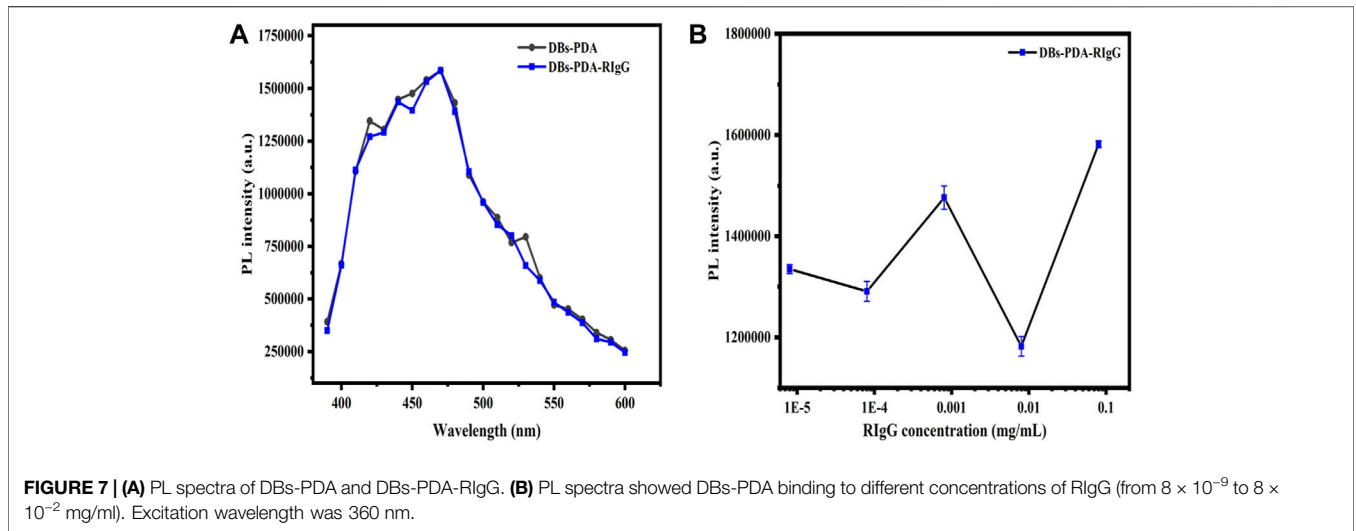
### 3.5 PL-Detection Compared With Fluorescence Immunoassay

Several studies have demonstrated the potential of the AuNP-based fluorescence-labeling probe technique applied on immunoassay and biosensors. The fluorescence spectra showed that GaR functionalized DBs-PDA and DBs-PDA-AuNPs and challenged with DyLight 488-RIgG concentrations ranging from  $8 \times 10^{-9}$  to  $8 \times 10^{-4}$  mg/ml. The fluorescence peak intensity was not proportional to the change of antigen DyLight 488-RIgG concentrations (Figures 9A,D). In addition, after binding with different DyLight 488-RIgG concentrations ranging from  $8 \times 10^{-9}$  to  $8 \times 10^{-4}$  mg/ml,



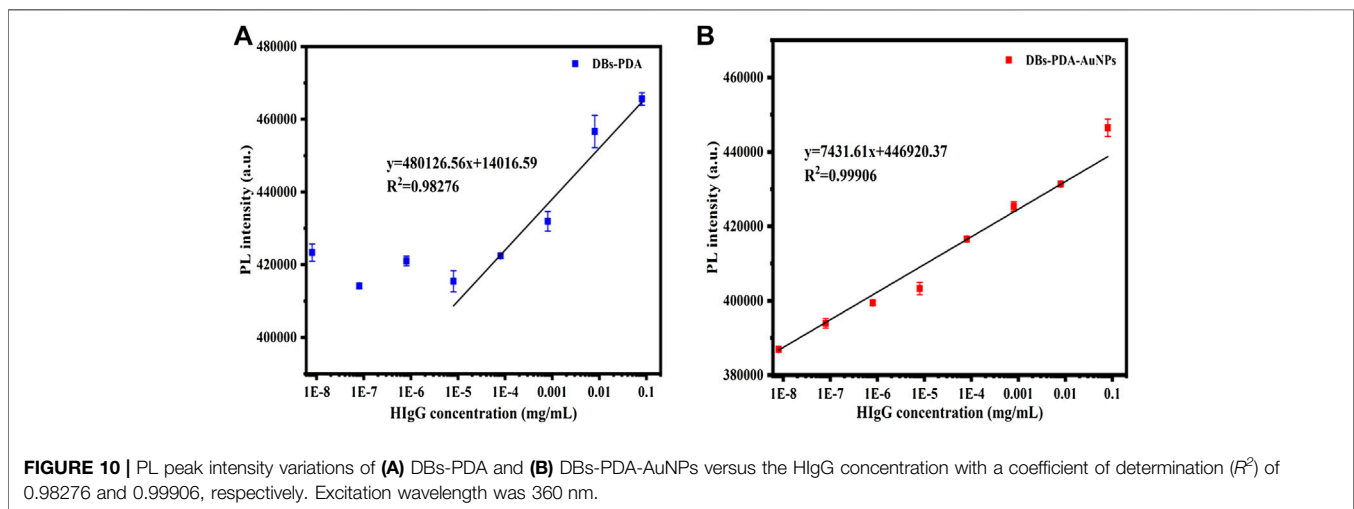
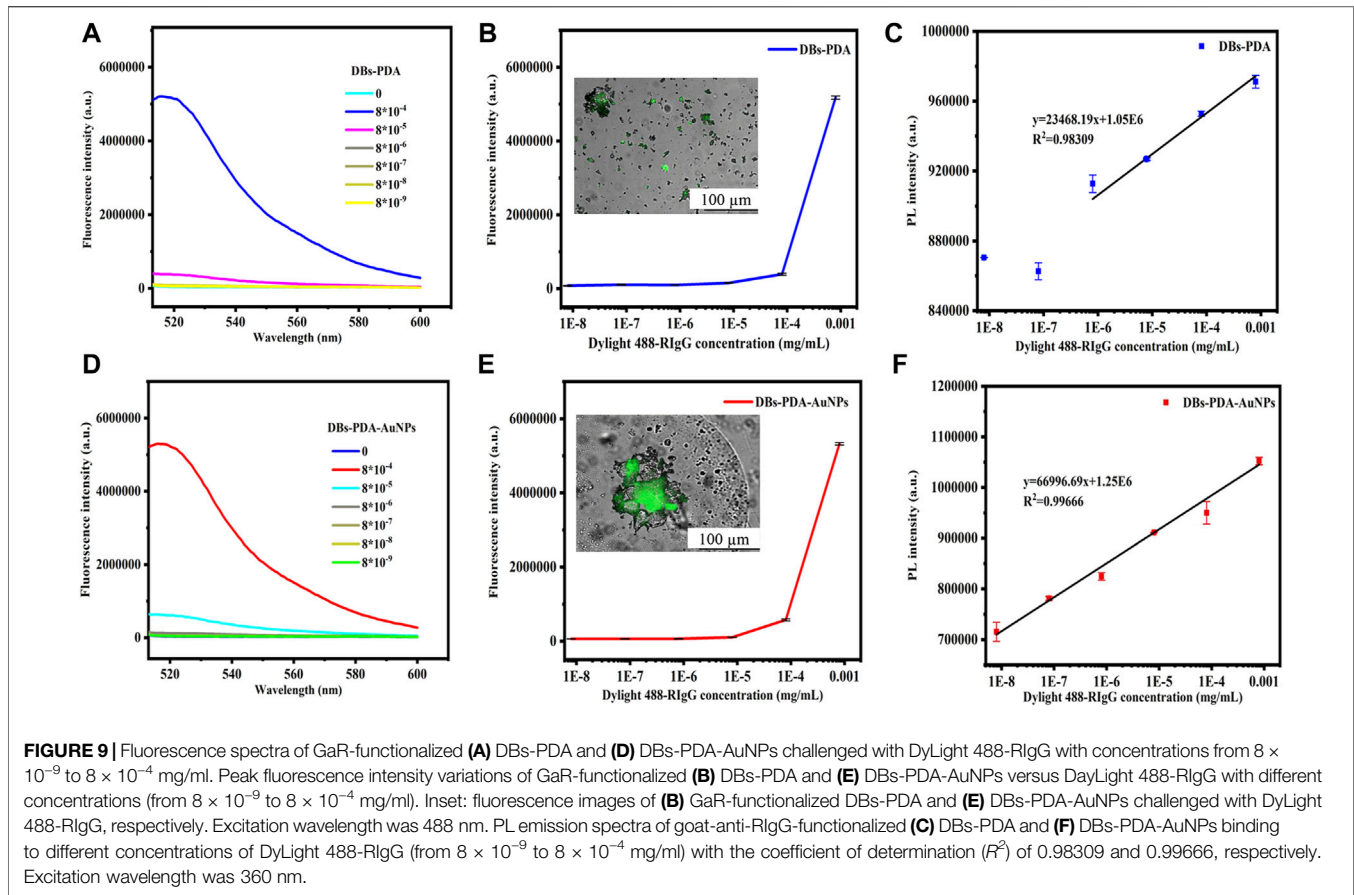
the fluorescence peak intensity was observed in fluorescence spectra. Two curves showed a similar variation trend and further indicated that there was no linear relation between fluorescence peak intensity and DyLight 488-RIGG concentrations. When challenged with RIGG-labeled DyLight 488, the entire surface of DBs-PDA and DBs-PDA-AuNPs both emitted green light which illustrated the successful binding

between DyLight 488-RIGG and GaR-functionalized DBs-PDA and DBs-PDA-AuNPs, respectively (**Figures 9B,E**, Inset). With the increase of DyLight 488-RIGG concentrations from  $8 \times 10^{-9}$  to  $8 \times 10^{-4}$  mg/ml, the PL peak intensity of DBs-PDA was found increasing linearly over a range from  $8 \times 10^{-9}$  to  $8 \times 10^{-4}$  mg/ml. The regression equation was  $y = 23468.19x + 1.05E06$  with the coefficient of determination



( $R^2$ ) of 0.98309 (**Figure 9C**). The correlation of DBs-PDA-AuNPs-GaR versus different concentrations of antigen DyLight 488-RlgG could be found in the PL spectrum. The

peak intensity of PL was observed increasing linearly with RlgG concentrations over a range from  $8 \times 10^{-9}$  to  $8 \times 10^{-4}$  mg/ml. The regression equation was  $y = 66996.69x + 1.25E06$  with the



coefficient of determination ( $R^2$ ) of 0.99666 (**Figure 9F**). The limit of PL detection for DyLight 488-RlgG based on DBs-PDA-AuNPs was three orders of magnitude higher than that based on DBs-PDA. Furthermore, the PL detection was more suitable in selective and quantitative detection of antigen DyLight 488-RlgG than fluorescence immunoassay.

### 3.6 HlgG Detection Based on DBs-PDA-AuNPs

The PL detection for HlgG was conducted to validate the universality of DBs-PDA and DBs-PDA-AuNPs as label-free optical biosensors for immune-detection. The increase in PL peak intensity of RaH-functionalized DBs-PDA-AuNPs (DBs-

PDA-AuNPs-RaH) with antigen HIgG concentrations ranged from  $8 \times 10^{-9}$  to  $8 \times 10^{-2}$  mg/ml was displayed. The PL peak intensity was found increasing linearly over a wide range from  $8 \times 10^{-9}$  to  $8 \times 10^{-2}$  mg/ml. The regression equation was  $y = 7,431.61x + 4.47E05$  with the correlation coefficient of determination ( $R^2$ ) of 0.99906 (Figure 10B). The LOD of DBs-PDA-AuNPs could reach  $8 \times 10^{-9}$  mg/ml. With the increase of HIgG concentrations, the PL peak intensity was linearly related to the concentration of HIgG concentrations from  $8 \times 10^{-6}$  to  $8 \times 10^{-2}$  mg/ml with the regression equation of  $y = 480126.56x + 1.40E04$  and the correlation coefficient ( $R^2$ ) of 0.98276 (Figure 10A). The LOD for HIgG detection based on DBs-PDA was three orders of magnitude lower than DBs-PDA-AuNPs. This result suggested that DBs-PDA-AuNPs were more suitable for quantitative detection of HIgG concentrations. Furthermore, PL detection based on DBs-PDA-AuNPs had the universality to be applied for immune detection in clinical samples.

## 4 CONCLUSION

In this present work, DBs obtained from the centric diatom *C. cryptica* were employed to establish a nanostructured immune assay platform coated with PDA and functionalized *via* AuNPs, which induced the decrease of defect concentration and quenched the PL peak intensity of DBs. N-Au formed after AuNPs reacted with PDA and further enhanced the surface passivation of DBs, which amplified the PL peak intensity of DBs-PDA-AuNPs as compared to DBs-PDA. The PL detection for RIgG based on DBs-PDA and DBs-PDA-AuNPs all exhibited high biological specificity. Nucleophilic complex formation increased the PL peak intensity of DBs-PDA and DBs-PDA-AuNPs. Furthermore, physisorption between antibody and DBs-PDA-AuNPs was likely to concentrate plenty of complimentary

antigens on the surface, which resulted in high sensitivity and a decrease in the LOD. The LOD of PL detection for RIgG and HIgG based on DBs-PDA-AuNPs could reach  $8 \times 10^{-9}$  mg/ml, which was three orders of magnitude higher than that of DBs-PDA. In addition, PL detection for DyLight 488-RIgG based on DBs-PDA-AuNPs exhibited higher LOD than fluorescence immunoassay. As such, antibody-functionalized DBs-PDA-AuNPs could serve as an efficient optical biosensor platform for the selective, sensitive, and label-free PL-based immunoassay.

## DATA AVAILABILITY STATEMENT

The original contributions presented in the study are included in the article/Supplementary Material; further inquiries can be directed to the corresponding author.

## AUTHOR CONTRIBUTIONS

All the authors contributed to the research. TC performed research, analyzed data and prepared figures; YL, FW, and HR performed research; XC and CF conceived and designed the study.

## FUNDING

The work was supported by the National Natural Science Foundation of China (Nos. 82172095 and 81801846), the Shandong Provincial Natural Science Foundation, China (No. ZR2019QD005), the Qingdao Science and Technology Demonstration and Guidance Project (20-3-4-50-nsh), and the Taishan Scholar Program.

## REFERENCES

- Artega-Larios, N. V., Nahmad, Y., Navarro-Contreras, H. R., Encinas, A., and Viridiana Garcia-Meza, J. (2014). Photoluminescence Shift in Frustules of Two Pennate Diatoms and Nanostructural Changes to Their Pores. *Luminescence* 29 (8), 969–976. doi:10.1002/bio.2646
- De Stefano, L., Rotiroli, L., De Stefano, M., Lamberti, A., Lettieri, S., Setaro, A., et al. (2009). Marine Diatoms as Optical Biosensors. *Biosens. Bioelectron.* 24 (6), 1580–1584. doi:10.1016/j.bios.2008.08.016
- De Tommasi, E. (2016). Light Manipulation by Single Cells: The Case of Diatoms. *J. Spectrosc.* 2016, 1–13. doi:10.1155/2016/2490128
- De Tommasi, E., Rea, I., De Stefano, L., Dardano, P., Di Caprio, G., Ferrara, M., et al. (2013). "Optics With Diatoms: Towards Efficient, Bioinspired Photonic Devices at the Micro-scale," in *Spie Optical Metrology*, Munich, Germany. 8792, 87920O. doi:10.1117/12.2021613
- Dong, Y.-L., Jiang, T., Xia, W., Dong, H.-P., Lu, S.-H., and Cui, L. (2015). Light Harvesting Proteins Regulate Non-photochemical Fluorescence Quenching in the Marine Diatom *Thalassiosira Pseudonana*. *Algal Res.* 12, 300–307. doi:10.1016/j.algal.2015.09.016
- Fedorenko, V., Viter, R., Mrówczyński, R., Damberga, D., Coy, E., and Iatsunskyi, I. (2020). Synthesis and Photoluminescence Properties of Hybrid 1D Core-Shell Structured Nanocomposites Based on ZnO/polydopamine. *RSC Adv.* 10 (50), 29751–29758. doi:10.1039/d0ra04829a
- Gale, D. K., Gutu, T., Jiao, J., Chang, C.-H., and Rorrer, G. L. (2009). Photoluminescence Detection of Biomolecules by Antibody-Functionalized Diatom Biosilica. *Adv. Funct. Mat.* 19 (6), 926–933. doi:10.1002/adfm.200801137
- Gordon, R., Losic, D., Tiffany, M. A., Nagy, S. S., and Sterrenburg, F. A. S. (2009). The Glass Menagerie: Diatoms for Novel Applications in Nanotechnology. *Trends Biotechnol.* 27 (2), 116–127. doi:10.1016/j.tibtech.2008.11.003
- He, N., Ge, S., Yang, C., Hu, C., and Gu, M. (2004). Investigation on the Mechanism of the Photoluminescence of MCM-41. *Mater. Res. Bull.* 39 (12), 1931–1937. doi:10.1016/j.materresbull.2004.05.018
- Jia, M., Shen, Y., Li, C., Bao, Z., and Sheng, S. (2005). Effect of Supports on the Gold Catalyst Activity for Catalytic Combustion of CO and HCHO. *Catal. Lett.* 99 (3–4), 235–239. doi:10.1007/s10562-005-2129-1
- Kashif, M., Majeed, M. I., Hanif, M. A., and Rehman, A. u. (2020). Surface Enhanced Raman Spectroscopy of the Serum Samples for the Diagnosis of Hepatitis C and Prediction of the Viral Loads. *Spectrochimica Acta Part A Mol. Biomol. Spectrosc.* 242, 118729. doi:10.1016/j.saa.2020.118729
- Lai, G., Zhang, H., Yong, J., and Yu, A. (2013). *In Situ* deposition of Gold Nanoparticles on Polydopamine Functionalized Silica Nanosphere for Ultrasensitive Nonenzymatic Electrochemical Immunoassay. *Biosens. Bioelectron.* 47, 178–183. doi:10.1016/j.bios.2013.03.029
- LeDuff, P., Roesijadi, G., and Rorrer, G. L. (2016). Micro-photoluminescence of Single Living Diatom Cells. *Luminescence* 31 (7), 1379–1383. doi:10.1002/bio.3118

- Leng, C., Lai, G.-S., Yan, F., and Ju, H.-X. (2010). Gold Nanoparticle as an Electrochemical Label for Inherently Crosstalk-free Multiplexed Immunoassay on a Disposable Chip. *Anal. Chim. Acta* 666 (1-2), 97–101. doi:10.1016/j.aca.2010.03.060
- Lin, H., Li, L., Lei, C., Xu, X., Nie, Z., Guo, M., et al. (2013). Immune-independent and Label-free Fluorescent Assay for Cystatin C Detection Based on Protein-Stabilized Au Nanoclusters. *Biosens. Bioelectron.* 41, 256–261. doi:10.1016/j.bios.2012.08.030
- Liu, Y.-S., Lin, H.-C., and Xu, H.-L. (2018). The Surface Plasmon Resonance Effect on the Defect-Mode Cholesteric Liquid Crystals Doped with Gold Nanoparticles. *IEEE Photonics J.* 10 (5), 1–7. doi:10.1109/jphot.2018.2821560
- Meyer, S. A., Le Ru, E. C., and Etchegoin, P. G. (2011). Combining Surface Plasmon Resonance (SPR) Spectroscopy with Surface-Enhanced Raman Scattering (SERS). *Anal. Chem.* 83 (6), 2337–2344. doi:10.1021/ac103273r
- Mishra, M., Singh, S. K., Bhardwaj, A., Kumar, L., Singh, M. K., and Sundaram, S. (2020). Development of a Diatom-Based Photoluminescent Immunosensor for the Early Detection of Karnal Bunt Disease of Wheat Crop. *ACS OMEGA* 5 (14), 8251–8257. doi:10.1021/acsomega.0c00551
- Peltomaa, R., Glahn-Martínez, B., Benito-Peña, E., and Moreno-Bondi, M. (2018). Optical Biosensors for Label-free Detection of Small Molecules. *Sensors* 18 (12), 4126. doi:10.3390/s18124126
- Petzold, A., and Zollfrank, C. (2019). A Facile Route to Diatoms Decorated with Gold Nanoparticles and Their Optical Properties. *Bioinspired, Biomim. Nanobiomaterials* 8 (1), 81–85. doi:10.1680/jbibn.18.00003
- Qin, T., Gutu, T., Jiao, J., Chang, C.-H., and Rorrer, G. L. (2008). Photoluminescence of Silica Nanostructures from Bioreactor Culture of Marine Diatom *Nitzschia Frustulum*. *J. Nanosci. Nanotechnol.* 8 (5), 2392–2398. doi:10.1166/jnn.2008.241
- Rea, I., Terracciano, M., Chandrasekaran, S., Voelcker, N. H., Dardano, P., Martucci, N. M., et al. (2016). Bioengineered Silicon Diatoms: Adding Photonic Features to a Nanostructured Semiconductive Material for Biomolecular Sensing. *Nanoscale Res. Lett.* 11 (1), 405. doi:10.1186/s11671-016-1624-1
- Ren, F., Campbell, J., Wang, X., Rorrer, G. L., and Wang, A. X. (2013). Enhancing Surface Plasmon Resonances of Metallic Nanoparticles by Diatom Biosilica. *Opt. Express* 21 (13), 15308. doi:10.1364/oe.21.015308
- Rorrer, G., Jeffryes, C., Chang, C., Lee, D., Gutu, T., Jiao, J., et al. (2007). “Biological Fabrication of Nanostructured Silicon-Germanium Photonic Crystals Possessing Unique Photoluminescent and Electroluminescent Properties,” in Proceedings of Spie the International Society for Optical Engineering, San Diego, CA. 6645, 66450A. doi:10.1117/12.735365
- Uram, J. D., Ke, K., Hunt, A. J., and Mayer, M. (2006). Label-Free Affinity Assays by Rapid Detection of Immune Complexes in Submicrometer Pores. *Angew. Chem.* 118 (14), 2339–2343. doi:10.1002/ange.200502862
- Uthappa, U. T., Kigga, M., Sriram, G., Ajeya, K. V., Jung, H.-Y., Neelgund, G. M., et al. (2019). Facile Green Synthetic Approach of Bio Inspired Polydopamine Coated Diatoms as a Drug Vehicle for Controlled Drug Release and Active Catalyst for Dye Degradation. *Microporous Mesoporous Mater.* 288, 109572. doi:10.1016/j.micromeso.2019.109572
- Viji, S., Anbazhagi, M., Ponpandian, N., Mangalaraj, D., Jeyanthi, S., Santhanam, P., et al. (2014). Diatom-based Label-free Optical Biosensor for Biomolecules. *Appl. Biochem. Biotechnol.* 174 (3), 1166–1173. doi:10.1007/s12010-014-1040-x
- Wang, Z., Xianyu, Y., Liu, W., Li, Y., Cai, Z., Fu, X., et al. (2019). Nanoparticles-Enabled Surface-Enhanced Imaging Ellipsometry for Amplified Biosensing. *Anal. Chem.* 91 (10), 6769–6774. doi:10.1021/acs.analchem.9b00846
- Xie, Y. H., Wilson, W. L., Ross, F. M., Mucha, J. A., Fitzgerald, E. A., Macaulay, J. M., et al. (1992). Luminescence and Structural Study of Porous Silicon Films. *J. Appl. Phys.* 71 (5), 2403–2407. doi:10.1063/1.351097
- Yang, H.-C., Liao, K.-J., Huang, H., Wu, Q.-Y., Wan, L.-S., and Xu, Z.-K. (2014). Mussel-inspired Modification of a Polymer Membrane for Ultra-high Water Permeability and Oil-In-Water Emulsion Separation. *J. Mat. Chem. A* 2 (26), 10225–10230. doi:10.1039/c4ta00143e
- Zhen, L., Ford, N., Gale, D. K., Roesijadi, G., and Rorrer, G. L. (2016). Photoluminescence Detection of 2,4,6-trinitrotoluene (TNT) Binding on Diatom Frustule Biosilica Functionalized with an Anti-TNT Monoclonal Antibody Fragment. *Biosens. Bioelectron.* 79, 742–748. doi:10.1016/j.bios.2016.01.002

**Conflict of Interest:** The authors declare that the research was conducted in the absence of any commercial or financial relationships that could be construed as a potential conflict of interest.

**Publisher’s Note:** All claims expressed in this article are solely those of the authors and do not necessarily represent those of their affiliated organizations, or those of the publisher, the editors, and the reviewers. Any product that may be evaluated in this article, or claim that may be made by its manufacturer, is not guaranteed or endorsed by the publisher.

Copyright © 2022 Chen, Wu, Li, Rozan, Chen and Feng. This is an open-access article distributed under the terms of the Creative Commons Attribution License (CC BY). The use, distribution or reproduction in other forums is permitted, provided the original author(s) and the copyright owner(s) are credited and that the original publication in this journal is cited, in accordance with accepted academic practice. No use, distribution or reproduction is permitted which does not comply with these terms.